Original article

Studies on physicochemical and antibacterial deeds of amino acid based L-Threoninum sodium bromide

S.V. Ashvin Santhia [a,*], B. Aneeba [a], S. Vinu [b], R. Sheela Christy [a], Amal M. Al-Mohaimeed [c], Dunia A. Al Farraj [d]

[a] Department of Physics and Research Centre, Nesamony Memorial Christian College, Marthandam, Affiliated to Manonmaniam Sundaranar University, Abishekapatti Tirunelveli, Tamil Nadu, India
[b] Department of Physics, Government Arts and Science College, Nagercoil, India
[c] Department of Chemistry, College of Science, King Saud University, P.O. Box 22452, Riyadh 11495, Saudi Arabia
[d] Department of Botany and Microbiology, College of Science, King Saud University, Riyadh 11451, Saudi Arabia

ABSTRACT

Highly translucent nonlinear single crystals of L-Threoninum Sodium Bromide (LTSB) has been grown because of their rising need for everyday life and the XRD studies (PXRD and SXRD) solemnly affirmed the crystallinity and non-centrosymmetric space group of LTSB materials. The bonding nature and diverse functional groups in LTSB were demonstrated by FTIR analysis when they absorb infrared radiation. The optical behavior of LTSB crystals was explored through UV–Vis spectroscopy, which shows optical parameters depend on photon energy with band gap E_g = 5.7 eV which was suitable for optoelectronic devices. The electrical properties of LTSB crystals were measured by using dielectric measurement. The solid state parameters of LTSB crystal were calculated. An antibacterial activity developed by LTSB crystals against different pathogenic bacteria were examined using the Agar disk diffusion process. The antibacterial inhibitory activity of LTSB crystal revealed that it can be used to treat a variety of bacterial infections.

1. Introduction

Currently, NLO crystals play a key role in view of the growing demand for their potential application in everyday life such as laser and light diversification, interactions with materials, information technology, and so on (Uma and Rajendran, 2016). Materials used for the above application must be of high transparency, low dielectric loss, and high efficiency of SHG (Martin Britto Dhas and Natarajan, 2007). At presents amino acid-based materials are given preeminence in several NLO optical applications, for the reason that it comprises profusions of optically active atoms that show highly frequency doubling efficiency and are effective for NLO applications (Kanika Thukral et al., 2019). Amino acid possesses

both acidic (–COOH) and basic (–NH$_2$) groups in the same molecule. These groups interact with each other and therefore amino acids possess double charge. This state is known as zwitterion or dipolar ion (Suresh and Sagadevan, 2014). In the zwitterionic state, the amino acids are electrically neutral and bear no net charge, which may produce an added betterment in nonlinear polarization (Bhuvaneswari and Nalini Jayanti, 2018). In contrast to other amino acids, L threonine is an essential amino acid to treat various nervous system disorders. It is used as an additive in manufacturing or as a substrate for the biosynthesis of other chemicals (Xunyan Dong et al., 2012). Thus L-threonine ($C_4H_9NO_3$) deserves higher optical properties and any applications than that of other amino acids (Rodriguesjr et al., 2003; Ramasamy and Meenakshisundaram, 2014). Sodium bromide is the most useful inorganic bromide in industry also it is used in medicine, preparation of other bromine compounds, disinfectant, and petroleum industry (Ward et al., 1978).

In this present manuscript LTSB crystal synthesized by a familiar slow evaporation technique and described their physicochemical properties. The novelty of this article is that an antibacterial activity developed from LTSB crystal against various pathogenic

bacteria has been studied using the Agar disk diffusion process. The zones for growth inhibition were measured in diameter (mm).

2. Synthesis, characterization and biological application

2.1. Material synthesis

Nonlinear single crystal of L-Threonine Sodium Bromide (LTSB) has been grown from the following highly purified chemicals given in the equation were purchased from Sigma-Aldrich and the solution was well stirred at 40 °C for nearly 3 h to obtain a saturated aqueous solution.

$$C_4H_9NO_3 + NaBr \rightarrow [C_4H_9NO_3Na^+] \, Br^-$$
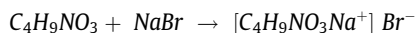
The prepared solution was filtered for extraction of impurities. The solution thus prepared was covered by porous perforated foil and kept undisturbed condition for evaporation. Extremely transparent nonlinear single LTSB crystal was harvested after 25–30 days as depicted in Fig. 1.

2.2. Characterization techniques

The unit cell parameters of the titular crystals were carried out using Bruker Kappa APEXII X-ray diffractometer. The crystallinity of LTSB crystal was checked by taking the Powder X-Ray diffraction using an XPERT-PRO diffractometer with Cu kα radiation (λ = 1.5 406 Å). The LTSB crystal's FT-IR spectrum was taped by Thermo Nicolet Avatar 370 spectrometer in the frequency region 400–4000 cm^{-1}. The UV–Vis spectrum of LTSB crystal was measured in the range of 200–800 nm by UV-1700 Series Spectrophotometer. The dielectric behavior is studied by using the Tonghui TH2826 Precision LCR Meter. The Agar disk diffusion method was employed to determine the antibacterial activities of grown LTSB crystal.

2.3. Biological application

An antibiotic resistance developed from LTSB crystal against 3 different pathogenic bacteria has been studied using the Agar disk diffusion process. The inhibitory activity produced by LTSB crystals were measured in diameter (mm).

3. Results and discussion

3.1. Single crystal X-ray diffraction analysis (SXRD)

To determine unit cell parameters, crystal system, and space group of the grown LTSB crystals were collected by using SXRD analysis with MoKα radiation of wavelength λ = 0.71073 Å. The space group which is required for SHG application is non-centrosymmetric space group P2$_1$2$_1$2$_1$. This space group of LTSB crystal was confirmed by SXRD analysis. From the collected data LTSB single crystal having three unequal cell parameters a = 5.15 Å, b = 7.74 Å, c = 13.61 Å, holding angles of 90^0 between them
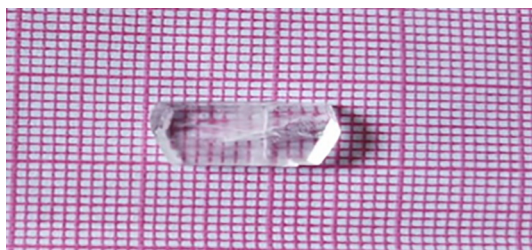

Fig. 1. Photograph of LTSB single crystal.

and cell volume 543 Å^3 confirms the LTSB crystal unambiguously the orthorhombic system, which shows a suitable concord with the reported literature (Allen Moses et al., 2019a, 2019b).

3.2. Powder X-ray diffraction analysis (PXRD)

PXRD analyses of LTSB crystal were carried out by crushing the defect free LTSB crystal into a fine powder. The LTSB samples were scanned for 2θ values from 10-80^0 is shown in Fig. 2. The crystalline characters with phase purity of the grown LTSB crystal were confirmed by most intense Bragg's reflection peaks appear at specific 2θ angles. The measured cell parameters from PXRD well agreed with single SXRD.

3.3. FTIR analysis

Vibrational spectroscopy employed to analyze the bonding structure and the diverse functional groups present in the unknown compound, reason that it is a nimble process without monotonous assessment methods. Moreover, the FTIR technique is beneficial in the identification of chemicals that are either organic or inorganic. Here FT-IR spectrum of LTSB sample in the 400–4000 cm^{-1} frequency region is shown in Fig. 3. To examine the received FTIR spectrum of LTSB crystal some amine and carboxylate groups are present, which confirms the zwitterionic nature of the LTSB crystal and it is a sinewy material for diverse applications. The wavenumbers observed and the proposed assignments of the LTSB crystal FTIR spectrum band are given in Table 1. FTIR assignment of LTSB crystal well agreed with the literature (Abila et al., 2020; Masilamani et al., 2017).

3.4. UV–Visible spectral analysis

UV–Vis spectroscopy analysis is a key factor for characterizing the feature of NLO. In order to examine the optical characteristics of the LTSB crystal, optical constants were playing a prominent role it is used for the application of optoelectronics and photonics (Hanumantharao and Kalainathan, 2012). The high transparency nature of the material also provides various information about electronic optical transition (Karuppasamy et al., 2020; Subhashini et al., 2019).

The transmittance spectrum of LTSB crystal in Fig. 4a shows a wide translucency window from 235 to 800 nm with 83% transmittance and no absorbance in the entire wavelength. In the absence of strong conjugated bonds in amino acid generate lower cut-off wavelength (221 nm) and good optical transparency of the LTSB crystal, so that the title crystals were suitable for any applications
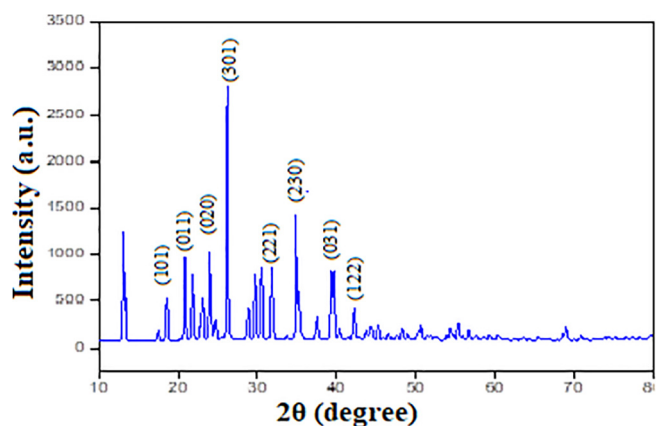

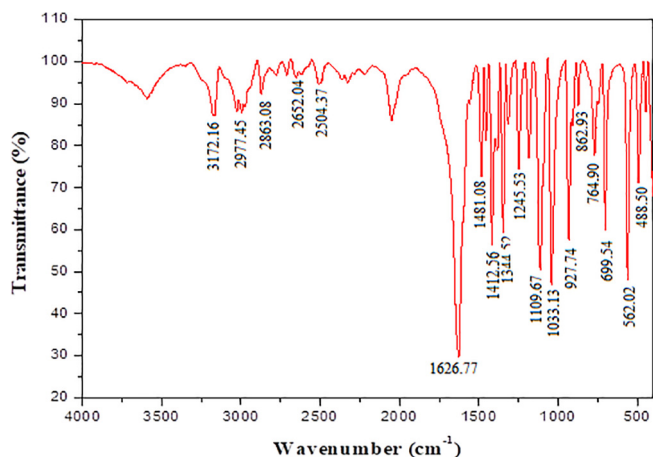**Fig. 2.** Powder XRD pattern of the LTSB crystal.

Fig. 3. FTIR spectra of LTSB crystal.

Table 1
FTIR assignments of the LTSB crystal.

| Wave number	Functional group
3172.16	NH^{3+} asymmetric stretching
2977.45	NH_3^+ stretching
2863.08	CH_3 symmetric stretching
2652.04	O-H stretching
2504.37	CH_3 stretching
1626.77	NH_3^+ asymmetric bending
1481.08	NH_3^+ symmetric bending
1412.56	CO2– symmetric stretching
1344.52	CH_3 bending
1317.70	CH_3 bending
1245.53	CH_3 bending
1109.67 and 1180. 18	NH_3 rocking
1033.13	C-N stretching
927.74	C-C stretching
862.93	CO_2 bending
764.90	COH torsion
699.54	CO_2^- Wagging vibration
562.02	C-C-N group deformation vibration
488.50	NH_3 torsional mode
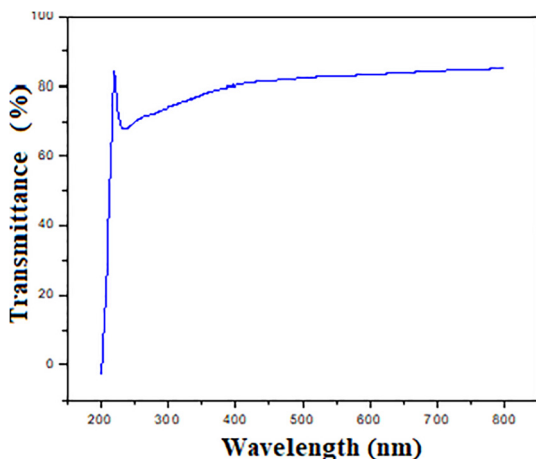
Fig. 4a. Transmission spectra of LTSB crystal.

(Tauc, 1972; Chennakrishnan et al., 2017). The optical absorption coefficient (α) and E_g according to Tauc's relationship is given in Eqs. (1) and (2):

$$\alpha = \frac{2.303}{t} \log \frac{1}{T} \qquad (1)$$

$$ah\upsilon = A(h\upsilon - E_g)^n \qquad (2)$$

Where all the symbols have their own significance

For LTSB crystal n = 1/2 indicated the direct band gap nature of the material (Ramanathan et al., 2005). Fig. 4b shows the graph between $(ah\upsilon)^2$ and $h\upsilon$ of LTSB crystal and the graph provides the value of energy gap of titular crystal. The extrapolation of the straight line to $(\alpha h\upsilon)^2 = 0$ yielded the value of $E_g = 5.7$ eV suggests titular crystal possesses dielectric nature and can be polarized under the influence of powerful radiation which is suitable for optical fabrication. The reflectance (R) and refractive indices (n) were calculated by Eqs. (3) and (4): (Allen Moses et al., 2019a, 2019b; Ollaa et al., 2019).

$$R = 1 \pm \frac{\sqrt{1 - exp(-\alpha t) + exp(\alpha t)}}{1 + \exp(-\alpha t)} \qquad (3)$$

$$n = -\frac{(R+1) \pm \sqrt{3R^2 + 10R - 3}}{2(R-1)} \qquad (4)$$

From Figs. 4c and 4d it is understood that the photon energy dependence of optical parameters (R and n) showing that these titular materials are apt for optoelectronic devices than the other crystals (Dillip et al., 2012). Fig. 4e suggests a small value of extinction coefficient in the lower energy region reveals the grown crystal permitting the free passage of electromagnetic radiation, while the high energy region indicates greater degrees of opacity. The coefficient of attenuation depends on the type of material and radiation intensity. A low extinction coefficient is apt for use as an optical material in processing devices. Skin depth is numerically define as,

$$\delta = \frac{1}{\alpha} \qquad (5)$$

Where δ is skin depth.

Fig. 4f shows when the photon energy is increased the skin depth also decreases for LTSB crystal. This result suggests the use of grown crystal for large range of optoelectronic applications.

3.5. Dielectric studies

To scrutinize the electrical properties and lattice dynamics, the grown material is subjected to dielectric measurements, for that the grown LTSB crystal is coated with graphite on opposite surfaces for creating a good conductive layer (Elberin et al., 2016; Revathi
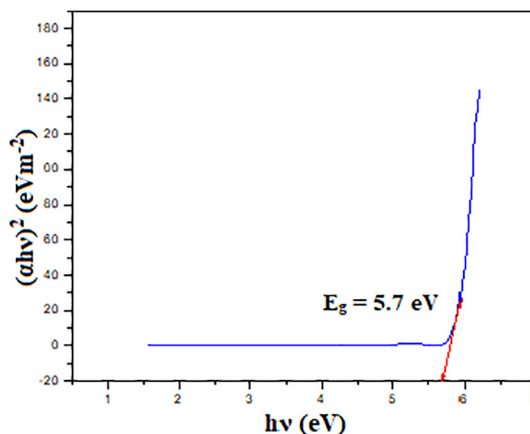

Fig. 4b. Plot of $(\alpha h\upsilon)^2$ versus Photon energy ($h\upsilon$).
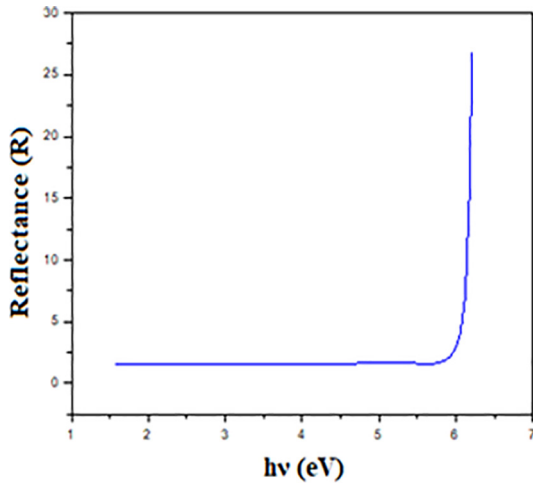
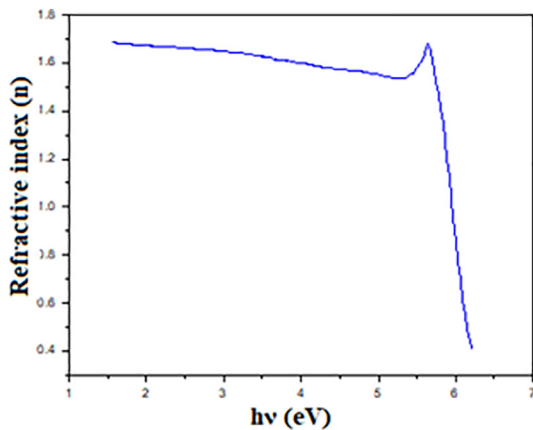**Fig. 4c.** Photon energy versus reflectance (d).

Fig. 4d. Photon energy versus refractive indices.
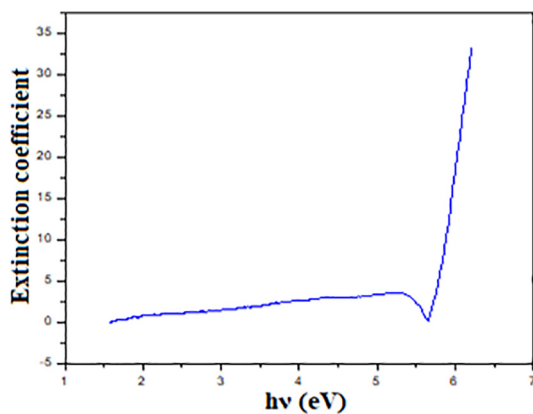

Fig. 4e. Extinction coefficient with photon energy.

and Rajendran, 2016). Herein the variation of capacitance and dissipation factor of the grown LTSB crystal measured in the frequency range of 100 Hz to 2 MHz and the temperatures from 313 to 433 K. The dielectric constant (ε_r) and dielectric loss (tanδ) were calculated by Eqs. (6) and (7) (Aneeba et al., 2020):

$$\varepsilon_r = \frac{Cd}{\varepsilon_0 A} \tag{6}$$
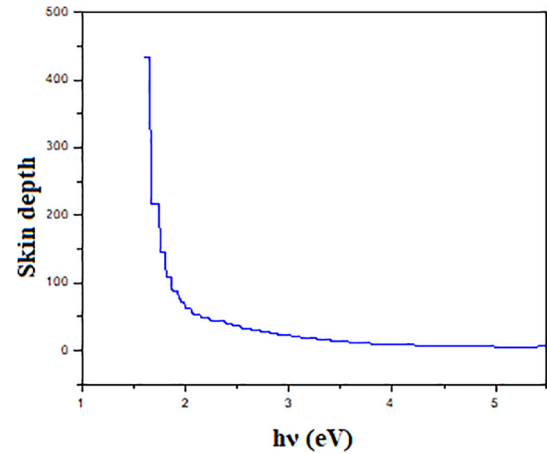

Fig. 4f. Skin depth of LTSB crystal.

$$tan\delta = \varepsilon_r D \tag{7}$$

Where all the symbols have their own significance.

Figs. 5a and 5b illustrates ε_r and tanδ of LTSB crystal against the frequency. It was observed from the graph that tanδ and ε_r decreased as the frequency increased and they being constant at higher frequencies due to predominant interfacial polarization near the grain boundary interfaces (Rao and Smakula,1966) moreover, this predominant interfacial polarization mainly depends on three factors specifically pureness, flawless and high temperature resistivity (Evangelin et al., 2020; HarshYadav et al., 2015). In that respect there are fewer defects and impurities are present in the grown LTSB crystal, and is used for NLO applications (Murugesan et al., 2020; Manoj Gupta et al., 2011). The AC conductivity (σ_{ac}) is obtained by Eq. (8):

$$\sigma_\alpha = \omega\varepsilon_0\varepsilon_r tan\delta \tag{8}$$

Fig. 5c illustrates the ac conductivity of titular material increases up to the logarithmic frequency of 5.78 Hz and also sharp increase was noted above 5.78 Hz that evidencing the conduction of the LTSB material.

3.6. Determination of solid state parameters

Electronic polarizability plays a decisive role in charge distribution of solids which, depending on some solid state parameters suchlike valance electron Plasma energy, Penn gap, Fermi energy,
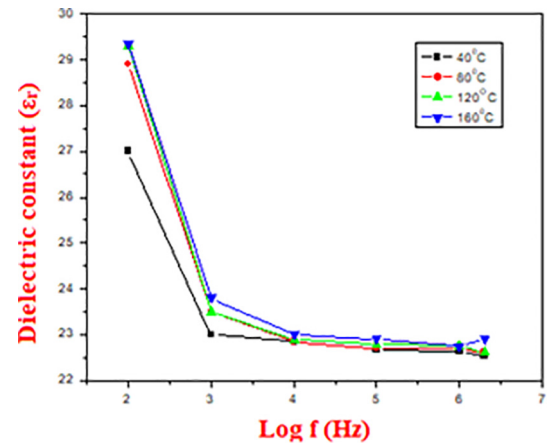

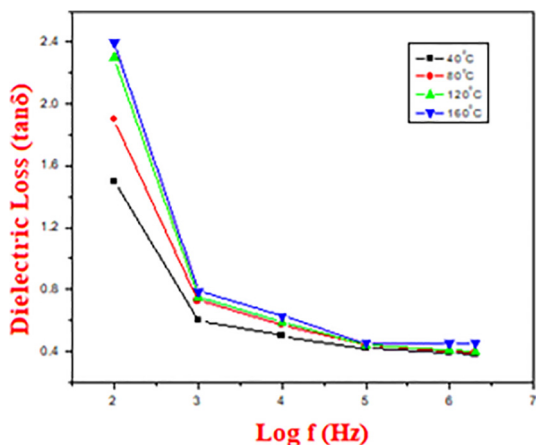**Fig. 5a.** Plot between dielectric constant and log f.

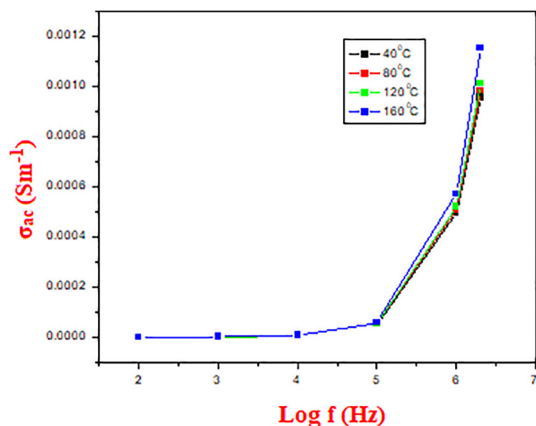**Fig. 5b.** Plot between dielectric loss and log f.

Fig. 5c. Plot between ac conductivity and log f.

and electronic polarizability are tabulated in Table 2. The valance electron plasma energy was evaluated by Eq. (9):

$$\hbar\omega_p = 28.8\left(\frac{Z\rho}{M}\right)^{1/2} \tag{9}$$

Where all the symbols have their own significance

The Pen gap energy (E_p) and Fermi energy (E_F) (Kalyanaraman et al., 2015) are expressed with the following relations

$$E_p = \frac{\hbar\omega_p}{\sqrt{\varepsilon_r - 1}} \tag{10}$$

$$E_F = 0.2948(\hbar\omega_p)^{4/3} \tag{11}$$

The polarizability α, from Penn gap analysis (Alexandar and Rameshkumar, 2018) is given by

$$\alpha = \left[\frac{(\hbar\omega_p)^2 S_0}{(\hbar\omega_p)^2 S_0 + 3E_P^2}\right] \times \frac{M}{\rho} \times 0.396 \times 10^{-24} \tag{12}$$

Where S_0 is the constant for given material

$$S_0 = 1 - \left[\frac{E_P}{4E_F}\right] + \frac{1}{3}\left[\frac{E_P}{4E_F}\right]^2 \tag{13}$$

The polarizability α is also be verified by using the Clausius-Mossotti relation (Umarani and Jagannathan, 2018) is given by

$$\alpha = \frac{3M}{4\pi N_A \rho}\left[\frac{\varepsilon_\infty - 1}{\varepsilon_\infty + 2}\right] \tag{14}$$

The obtained polarizability value of LTSB crystal using Penn analysis and Clausius-Mossotti relation are evenly matched.

3.7. Antibacterial study

The Agar disk diffusion method was used in order to ensure the antibacterial activities of grown LTSB crystal with aminoglycoside antibiotics class of Amikacin as a control (Xiaoting Wang et al., 2019). The basic principle behind this method is to estimate the antibiotic resistance by measuring the growth inhibition zone around the powered sample (Mahboobeh Maghami et al., 2015). Fig. 6(a, b and c) shows the inhibitory activity produced by LTSB crystals against 3 different pathogenic bacteria. The growth inhibition zones of the titular compounds were measured in diameter (mm) and the results are given in Table 3. From the results of

Table 2
Theoretical solid state parameters of LTSB crystal.

Parameters	Value
Plasma energy (eV)	15.84
Fermi energy (eV)	11.72
Penn energy (eV)	5.01
Polarizability from Penn analysis(cm)^3	6.07×10^{-23}
Polarizability from Clausius-Mossotti relation (cm)^3	5.73×10^{-23}

Table 3
The growth inhibition zones of LTSB crystal.

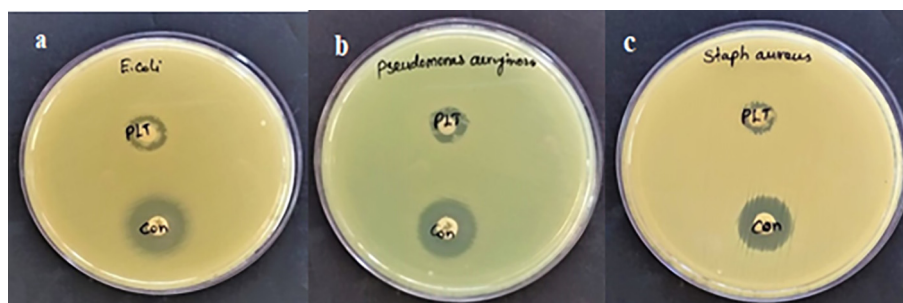| Bacterial strain		Control	Diameter of inhibition zone (mm)
Gram-negative	Escherichia coli	Amikacin	15
	Pseudomonas aeruginosa	Amikacin	13
Gram-positive	Staphylococcus aureus	Amikacin	12

Fig. 6. (a) ZOI of Escherichia coli (b) ZOI of Pseudomonas aeruginosa (c) ZOI of Staphylococcus aureus.

antibacterial activity studies, it was found that the prepared LTSB crystals are more toxic to Escherichia coli having a ZOI of 15 mm, and also the Gram-positive bacterial strains are less affected than gram-negative crystal. Thus LTSB crystal showed substantial antibacterial activity on Escherichia coli than (Huizhi Kou et al., 2020) also it has more inhibition effect on Pseudomonas aeruginosa and Staphylococcus aureus than the reported value of (M. Mayakannan et al., 2020; ChaoLiu et al., 2020). However, the antibacterial test demonstrates that LTSB crystal inhibits the growth of Escherichia coli, Pseudomonas aeruginosa and Staphylococcus aureus ergo the titular crystal can be used together with Amikacin to treat wide kind of bacterial infections.

4. Conclusion

The LTSB crystals were successfully grown and also the orthorhombic system belonging to non-centrosymmetric space group P2$_1$2$_1$2$_1$ of the LTSB was obtained by Single crystal XRD. The single crystalline characters of LTSB crystal were affirmed by powder XRD analysis. FTIR study has identified the different functional groups of LTSB crystal. The UV–Vis spectrum reveals the titular compound is active with 83% transmittance and the band gap E_g = 5.7 eV. For LTSB crystals the obtained polarizability value of Penn analysis and Clausius-Mossotti relation are evenly matched. The antibacterial inhibitory activity of LTSB crystal revealed that it can be used to treat a variety of bacterial infections. The findings from various studies suggest that the sample that was grown can be used for many applications.

Acknowledgement

References

Abila Jeba Queen, M., Bright, K.C., Mary Delphine, S., Aji Udhaya, P., 2020. Spectroscopic investigation of supramolecular organometallic compound L-threonine cadmium acetate monohydrate. Spectrochim. ActaPart A. 228, 117802.

Alexandar, A., Rameshkumar, P., 2018. Nucleation, growth, dielectric, polarizability, and Z-scan analysis of nicotinium tartrate & L-tartaric acid nicotinamide single crystals for third order NLO application: A comparative study. Optik. 168, 944–955.

Allen Moses, S.E., Tamilselvan, S., Ravi Kumar, S.M., Johnson, J., 2019a. Synthesis, Growth and characterization of semi-organic nonlinear optical L-threonium sodium fluoride (LTSF) crystal for photonics application. Chin. J. Phys. 58, 294–302.

Allen Moses, S.E., Tamilselven, S., Ravi Kumar, S.M., Vinitha, G., Hegde, Tejaswi Ashok, Vimalan, M., Varalakshmi, S., Sivaraj, S., 2019b. Synthesis, Growth and physicochemical properties of new organic nonlinear optical crystal L-threonium tartarate(LTT) for frequency conversion. Mater. Sci. Energy Technol. 2, 565–574.

Aneeba, B., Ashvin Santhia, S.V., Vinu, S., Sheela Christy, R., Al Farraj, Dunia A., Alkubaisi, Noorah A., 2020. Influence of most reactive inorganic cation in the optical and biological activities of L-Lysine monohydrochloride crystal.Saudi. J. Biol. Sci. 27, 2961–2967. https://doi.org/10.1016/j.sjbs.2020.07.018.

Bhuvaneswari, N., Nalini Jayanti, S., 2018. Effect of l-threonine on optical and electrical properties of TTZS crystal. Mater. Today. 5, 3378–3389.

Liu, Chao, Chen, Ming-Xing, Li, Ming, 2020. Synthesis, crystal structures, catalytic application and antibacterial activities of Cu(II) and Zn(II) complexes bearing salicylaldehyde-imine ligands. Inorganica Chim. Acta. 508, 119639.

Chennakrishnan, S., Ravi Kumar, S.M., Shanthi, R., Srineevasan, C., Kubendiran, T., Dsivavishnu, , Packiya Raj, M., 2017. Synthesis of the semi-organic nonlinear optical crystal L-glutamic acid chloride and investigation of its growth and physiochemical properties. J. Taibah. Univ. Sci. 11, 955–965.

Dillip, G.R., Bhagavannarayana, G., Raghavaiah, P., Deva Prasad Raju, B., 2012. Effect of magnesium chloride on growth, crystalline perfection, structural, optical,

thermal and NLO behavior of γ-glycine crystals. Mater. Chem. Phys. 134, 371–376.

Elberin Mary Theras, J., Kalaivani, D., Mercina, M., Jayaraman, D., Joseph, V., 2016. Characterization of L-threonine phthalate crystal for photonic and nonlinear optical applications. Optic. 127, 3397–3401.

Evangelin Teresa, P., Sornambol, M., Gowri, S., Aarthi, J., Navina, M., 2020. Growth, spectral, dielectric, magnetic and antimicrobial studies on dye doped rochelle salt crystal. Results Mater. 6, 100095.

Yadav, Harsh, Sinha, Nidhi, Kumar, Binay, 2015. Growth and characterization of new semiorganic nonlinear optical and piezoelectric lithium sulfate monohydrate oxalate single crystals. Mater. Res. Bull. 64, 194–199.

Kou, Huizhi, Wang, Yang, Ding, Peipei, Cheng, Xianzhong, Zhou, Guoqing, 2020. Synthesis, crystal structure, phosphate hydrolysis activity and antibacterial activity of macrocyclic dinuclear Zn(II) complex with benzyl pendant-arms. J. Mol. Struct. 1216, 128299.

Kalyanaraman, S., Shajinshinu, P.M., Vijayalakshmi, S., 2015. Refractive index, band gap energy, dielectric constant and polarizability calculations of ferroelectric Ethylenediaminium Tetrachlorozincate crystal. J. Phys. Chem. Solids. 86, 108–113.

Thukral, Kanika, Vijayan, N., Krishna, Anuj, Singh, Budhendra, Kant, Rajni, Jayaramakrishnan, V., Jayalakshmy, M.S., Kaur, Milanpreet, 2019. In-depth behavioral study of l-Prolinium Trichloroacetate single crystal: An efficient candidate for NLO applications. Arab. J. Chem. 12, 4887–4896.

Karuppasamy, P., Kamalesh, T., Anitha, K., Pandian, MuthuSenthil, Ramasamy, P., Verma, Sunil, 2020. Design and growth of novel organic molecular Quinoline 4-nitrophenol (QNP) single crystals: For Nonlinear optical (NLO) applications. J. Mol. Struct. 1210, 128036.

Maghami, Mahboobeh, Farzaneh, Faezeh, Simpson, Jim, Ghiasi, Mina, Azarkish, Mohammad, 2015. Synthesis, crystal structure, antibacterial activity and theoretical studies on a novel mononuclear cobalt(II) complex based on 2,4,6-tris(2-pyridyl)-1,3,5-triazine ligand. J. Mol. Struct. 1093, 24–32.

Manoj Gupta, K., Sinha, Nidhi, Kumar, Binay, 2011. Growth and characterization of new semi-organic L-proline strontium chloride monohydrate single crystals. Phys. B 406, 63–67.

Martin Britto Dhas, S.A., Natarajan, S., 2007. Growth and characterization of L-prolinium tartrate–A new organic NLO material. Cryst. Res. Technol. 42, 471–476.

Masilamani, S., Mohamed Musthafa, A., Krishnamurthi, P., 2017. Synthesis, growth and characterisation of a semiorganic nonlinear optical material: L-threonine cadmium chloride single crystals. Arab. J. Chem. 10, 3962–3966.

Mayakannan, M., Gopinath, S., Vetrivel, S., 2020. Synthesis and characterization of antibacterial activities nickel doped cobalt oxide nano particles. Mater. Chem. Phys. 242, 122282.

Murugesan, G., Nithya, R., Kalainathan, S., 2020. Colossal dielectric behaviour of Sr$_2$TiMnO$_{6-\delta}$ single crystals. J. Cryst. Growth. 530, 125179.

Mailoud, Ollaa M., Elsayed, Adly H., AbuEl Fetouh, H., Abu ELazm, A.H., 2019. Synthesis and characterization of paramagnetic isotropic glycine manganese chloride single crystal with various dopant concentrations. Results Phys. 12, 925–933.

Ramanathan Bairava Ganesh, Vasudevan Kannan, Meera, Narayana Perumal Rajesh, K., 2005. Synthesis, growth and characterization of a new nonlinear optical crystal sodium acid phthalate. J. Cryst. Growth. 282, 429–433.

Ramasamy, G., Meenakshisundaram, Subbiah, 2014. Studies on amino acid picrates: Crystal growth, structure and characterization of a new nonlinear optical material L-isoleucinium picrate. Optik. 125, 4422–4426.

Rao, K.V., Smakula, A., 1966. Dielectric properties of alkaline earth fluoride single crystals. Int. J. Appl. Phys. 37, 319–323.

Hanumantharao, Redrothu, Kalainathan, S., 2012. Growth, spectroscopy, dielectric and nonlinear optical studies of novel organic NLO crystal: L-Threonine formate. Spectrochim. Acta Part A. 94, 78–83.

Revathi, V., Rajendran, V., 2016. Investigation on growth and characteristics of undoped and Mn doped glycinium oxalate single crystals. Karbala Int. J. Mod. Sci. 2, 169–177.

Rodriguesjr, J.J., Misogutif, L., Nunesc, D., Mendonças, R., Zilio, C., 2003. Optical properties of L-threonine crystals. Opt. Mater. 22, 235–240.

Subhashini, R., Arunan, S., Gunasekaran, B., 2019. Synthesis of metal coordinated amino acid based nonlinear single crystal, Bis(L-threonine)zinc(II) using the solution growth technique and its physicochemical properties. J. Phys. Chem. Solids. 135, 109077.

Suresh, Sagadevan, 2014. Synthesis, growth and characterization of L-threonine zinc acetate (LTZA) NLO single crystal. Optik (Stuttg.) 125, 4547–4551.

Tauc, J., 1972. Optical Properties of Solids. J. Sci. Res. North Holland, Amsterdam.

Uma, J., Rajendran, V., 2016. Growth and properties of semi-organic nonlinear optical crystal L-Glutamic acid hydrochloride. Prog. Nat. Sci. 26, 24–31.

Umarani, P., Jagannathan, K., 2018. Growth, structural, thermal, dielectric and nonlinear optical properties of potassium hexachlo ro cadmate (IV) a novel single crystal. Phys. B 530, 215–221.

Ward, D.L., Wei, K.T., Hoogerheide, J.G., Popov, A.I., 1978. The crystal and molecular structure of the sodium bromide complex of monensin, C$_{36}$H$_{62}$O$_{11}$.Na$^+$Br$^-$. Acta Crystallogr B. 34, 110–115.

Wang, Xiaoting, Li, Ruiying, Liu, Aogang, Yue, Caipeng, Wang, Shimin, Cheng, Jiajia, Li, Jinpeng, Liu, Zhongyi, 2019. Syntheses, crystal structures, antibacterial activities of Cu(II) and Ni(II) complexes based on terpyridine polycarboxylic acid ligand. J. Mol. Struct. 1184, 503–511.

Dong, Xunyan, Quinn, Peter J, Wang, Xiaoyuan, 2012. Microbial Metabolic Engineering for L-Threonine Production. Subcell. Biochem. 64, 283–302.